Analysis of the RRKM Calculations in *J. Phys. Chem.* 1993, 97, 2, 385–390

https://doi.org/10.1021/j100104a020 Kameron Hansen

Section 1: Introduction

Reily and Baer (ref [1]) in their 1993 JPC paper used a technique called photoelectron-photoion coincidence spectroscopy (PEPICO) to experimentally measure the dissociation rate of dimethylformamide (DMF) cations.

In the researcher's PEPICO experiment, a DMF gas is leaked into the ultra-high vacuum chamber of a time of flight (TOF) mass spectrometer. The DMF molecules are then ionized by a continuous H_2 UV source whose low flux ensures that the molecules are ionized via a one-photon process. Upon ionization, the TOF mass spectrometer's potential gradient accelerates the electrons and ions in opposite directions. The electron's time of flight is three orders of magnitude shorter than the ion's time of flight. Therefore, the detection of the electrons marks $t = 0$ and the ion's delayed arrival Δt is measured on the opposite side of the chamber.

An ion's time of flight is inversely proportional to its acceleration through the electric field, where acceleration results from the Coulomb force of the chamber's electric field $a = \frac{q\,E}{m}$. Since E is the same for each particle, therefore, species of varying charge-to-mass ratio can be distinguished by their arrival time (time of flight) at the ion detector. By varying the photon energy, the researches could vary the internal energy imparted to the free DMF molecules. The DMF molecule's internal energy can be approximated as the difference between photon energy ($\hbar\omega$) and ionization potential (IP): $E_{internal} = \hbar\omega - IP$. Additional terms such as the photoelectron's kinetic energy and the internal energy of the neutral molecule prior to ionization

can be ignored due to their comparatively small magnitude. In order to assume a small neutral molecule internal energy, the researchers supersonically cooled the DMF gas, then used an effusive needle to record the thermal spectra and then subtracted out a 15% thermal background in the molecular beam data.

To determine how the dissociation products vary with internal energy, the researchers must first identify each peak in the TOF spectra. As seen in Fig 1. (a), a total of six peaks were resolved with m/z ratios of: 44, 58, 72, 73, 74, and 146, with the largest peak at m/z = 74 corresponding to the charge to mass ratio of a DMF molecule (m = 73 amu) of charge $+e$. By measuring the relative peaks height's dependence on the DMF gas' partial pressure (and overall peak shape), the researchers were able to determine which species of the remaining peaks (m/z = 44, 58, 72, 74) originated from DMF, the DMF dimer, or higher clusters. The 146 peak naturally corresponds to the DMF dimer. The peak heights for m/z = 44 and 58 varied consistently relative to the m/z = 73 DMF molecule. Whereas the m/z = 146 and 72 peaks decreased significantly with partial pressure suggesting that these peaks are the dissociation products of clusters larger than a dimer. Finally, the m/z = 74 peak increased, suggesting that it likely is the byproduct of the neutral dimer. The asymmetric broadening of the m/z = 44 and 58 peaks further corroborate their assignment to dissociation products of the DMF ion. The researchers used the asymmetric peak shapes (ref[1], Fig. 2) to extract the DMF ion dissociation rate constants k_{44} and k_{58} . By varying the photon energy, these rate constants were then plotted as a function of the ion internal energy (ref[1], Fig. 4). Since the peak shapes (m/z = 44 and 58) have similar asymmetry (and therefore similar rates), there must be a competitive dissociation into these products, i.e.

$$k_{eff} = k_{44} + k_{58}$$

Where k_{44} and k_{58} are:

$$(CH_3)_2NCHO^+ \xrightarrow{k_{44}} (CH_3)_2N^+ + CHO$$

$$(CH_3)_2NCHO^+ \xrightarrow{k_{58}} CH_3NCHO^+ + CH_3$$

The neutrals CHO and CH_3 are not directly detected in the experiment. Rather, it is the charged remainder of DMF, i.e. $(CH_3)_2N^+$ (amu 44) and CH_3NCHO^+ (amu 58) that appear at m/z 44 and m/z 58, allowing researchers to infer the decay products CHO and CH_3, respectively.

These experimental rate constants were obtained at photon energies $\hbar\omega = \{11.11, 11.21, 11.27, 11.39, 11.49\}$ eV. Subtracting the ionization potential of the DMF molecule, 9.13 eV, the resulting DMF cations were assumed to have internal energies $E_{int} = \{1.98, 2.08, 2.14, 2.26, 2.36\}$ eV. Using only one fit parameter of E_0 for the barrier height, these experimental values of $k(E)$ for both the CHO and CH_3 decay processes were fit to a theoretical RRKM curve based on the function:

$$k(E) = \frac{\sigma \int_E^{E_{int}-E_0} \rho^{\pm}(E_{int} - E_0 - \varepsilon)\, d\varepsilon}{h\, \rho(E_{int})}$$

Where σ is the symmetry number, ε is the energy in the critical coordinate at the transition state, and $\rho^{\pm}$ and ρ are the vibrational density of states for the transition states and molecular ion, respectively. Performing the fit, researchers determined the barrier heights of the CHO and CH_3 decay processes to be $E_{0,44} = 1.60\ eV$ and $E_{0,58} = 1.68\ eV$, respectively.

An inverse Laplace transform of the vibrational partition function for the transition state and DMF molecular ion were used to calculate $\rho^{\pm}$ and ρ, using the algorithm of steepest decent. The vibrational frequencies were obtained from ab initio unrestricted Hartree Fock (HF) calculations using a 3-21 G* basis set. Transition states were identified by locating saddle points in the HF potential energy surface, i.e. $\frac{d^2E}{dr^2} > 0$. The two identified transitions states had 29 real

vibrational modes and one imaginary, whereas the molecular ion was found to have 30 real vibrational modes.

Section 2: Molecular parameters

Table 1: Vibrational mode energies for the CH_3 transition state, the CHO transition state, and the charged DMF molecule. All values obtained from ab initio calculations in ref [1].

CHO Transition State (TS1) vibrational energies (cm^{-1})	CH_3 Transition State (TS2) vibrational energies (cm^{-1})	DMF Cation vibrational energies (cm^{-1})
3099	2986	3019
3002	2984	3006
2973	2965	2975
2971	2964	2951
2962	2880	2945
2890	2879	2878
1796	1750	2870
1471	1535	1473
1461	1467	1468
1439	1465	1450
1406	1456	1445
1380	1449	1437
1320	1435	1415
1240	1421	1367
1160	1219	1260
1135	1140	1176
1089	1118	1121
1014	1100	1086
954	921	1056
890	909	939
855	848	903
709	648	899
576	558	699
425	348	549
405	318	394
355	261	360

283	163	310
156	154	210
121	96	118
		85

Table 2: Molecular moments of inertia, calculated myself. The molecule drawing software 'iqmol' was used to mimic the three computationally-optimized structures in ref[1] Fig(3), the moments of inertia of the drawn structures were then computed with the Qchem set of programs.

	CHO Transition State (TS1)	CH_3 Transition State (TS2)	DMF Cation
I_A $(amu \cdot \dot{A}^2)$	59.6277608	74.2541348	55.7953857
I_B $(amu \cdot \dot{A}^2)$	126.110824	133.171816	122.004338
I_C $(amu \cdot \dot{A}^2)$	179.300819	183.847076	171.372853

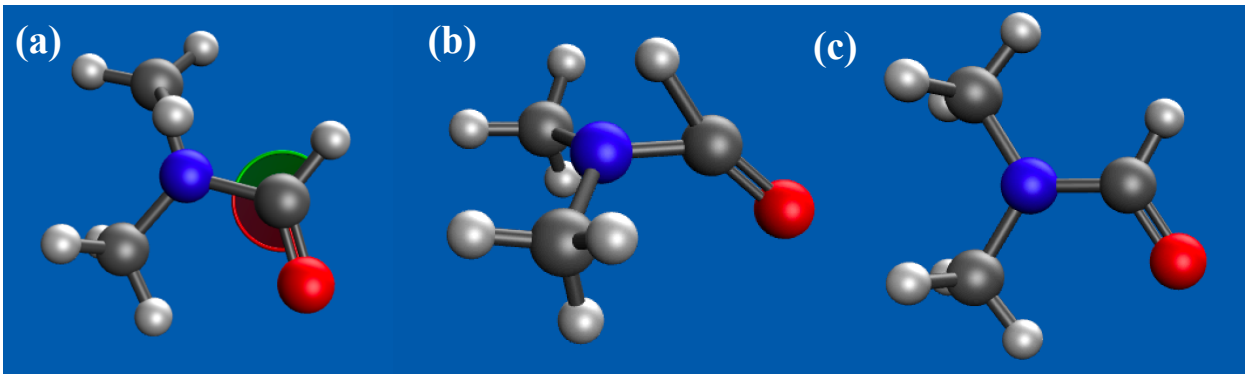

Figure 1: Structures used for moment of inertia calculations, (a) TS1 (b) TS2 and (c) DMF ion.

Section 3: Intermediate values

The rotational partition functions were calculated by inputting the values from Table 2 into:

$$Q_R = \frac{\sqrt{\pi}}{\sigma}\left(\frac{8\pi^2 k_B T}{h^2}\right)^{\frac{3}{2}} (I_A I_B I_C)^{1/2}$$

For $T = 50$ K and $\sigma = 1$.

	CHO Transition State (TS1)	CH_3 Transition State (TS2)	DMF Cation
Q_R	33851.4	39307.9	31487.9

For the Whitten-Rabinovitch method, some intermediate numbers are as follows:

E_{int} (cm^{-1})	TS1: $N^{\pm}(E - E_0)$	TS2: $N^{\pm}(E - E_0)$	DMF ion $\rho(E)$
15324.533	9965.98457861715	18234.4607262943	11890912901.3230
16050.432	72911.9587614426	106943.225960724	23729295416.2562
16856.986	505164.317598813	621597.189562166	49997644807.1936
17663.541	2846262.42531462	3067098.79430458	103045629011.490
18470.095	13714381.5683499	13303062.9903680	208041439174.694
19276.650	58369645.9020313	51944039.2147804	411975423894.452

For the Beyer-Swinehart direct counting algorithm, some intermediate numbers are as follows:

E_{int} (cm^{-1})	TS1: $N^{\pm}(E - E_0)$	TS2: $N^{\pm}(E - E_0)$	DMF ion $\rho(E)$
15325	6638	15126	11975000000
16050	54688	92922	23804050000
16857	410696	558039	50018040000
17664	2431865	2820481	102826600000
18470	12139340	12424130	206934200000
19277	52983310	49140800	408897100000

Section 4: Comparison of Results

I reproduced the theoretical $k(E)$ curves shown in ref[1] Fig. 4. Both the Whitten-Rabinovitch method and the Beyer-Swinehart direct-counting algorithm were implemented to calculate the total number of states above the transition barrier $N^{\pm}(E - E_0)$ as well as the DMF molecule's density of states $\rho(E)$.

$$k(E) = L^{\pm} \frac{Q_R^{\pm}}{Q_R} \frac{N^{\pm}(E - E_0)}{h\,\rho(E)}$$

Where the symmetry factor is unity ($L^{\pm} = 1$) for the molecules in this study. The barrier heights are $E_0 = 1.60$ and 1.68 for the respective CHO and CH_3 decay reactions.

Table 3: Comparison of $k_{eff}(E)$ values, WR/BS methods compared to experimental results in ref[1].

E_{int} (eV)	E_{int} (cm^{-1})	Experimental, ref[1]	WR method	BS method
1.98	15970	2.4 •10^5	2.38 •10^5	2.10 •10^5
2.08	16776	5.4 •10^5	7.15 •10^5	6.15 •10^5
2.14	17260	7.7 •10^5	1.28 •10^6	1.13 •10^6
2.26	18228	3.0 •10^6	3.57 •10^6	3.26 •10^6
2.36	19035	5.7 •10^6	7.54 •10^6	7.02 •10^6

Although my calculations deviate significantly from the reported values in ref [1] (Table 3), it is important to remember that these ref[1] values are measurements with high uncertainty. Unfortunately, the researchers did not tabulate the numerical results of their RRKM calculation of $k(E)$, therefore, a comparison between the RRKM calculations can only be done by eye. Looking at Fig. 2, all calculation methods produce very similar curves in an internal energy range spanning from 1.9 to 2.4 eV (15325 to 19357 cm^{-1}). Measuring the panel's (c) and (d) with a straight edge, the end points at 1.9 eV and 2.4 eV can be estimated by eye. These numbers are reported in the k_{44} (Panel c) and k_{58} (Panel d) columns in Table 4.

Table 4: Comparison of RRKM values for k_{44} and k_{58} values. The values in columns labeled "k_{44} (Panel c)" and "k_{58} (Panel d)" are rough estimates obtained by measuring the minimum and maximum values on the semi-log plot shown Figure 2.

E_{int} (eV)	**k_{44} (Panel c)**	**WR k_{44}**	**WR % difference**	**BS k_{44}**	**BS % difference**
1.9	3.9 •10^4	5.74 •10^4	32.2 %	4.73 •10^4	17.54 %
2.4	4.1 •10^6	5.10 •10^6	19.6 %	4.82 •10^6	14.9 %

E_{int} (eV)	**k_{58} (Panel d)**	**WR k_{58}**	**WR % difference**	**BS k_{58}**	**BS % difference**
1.9	1.8 •10^4	2.70 •10^4	33.1 %	1.79 •10^4	0.5 %
2.4	4.7 •10^6	4.89 •10^6	4.1 %	4.53 •10^6	3.8 %

CH_3 – TS2 – k_{44}

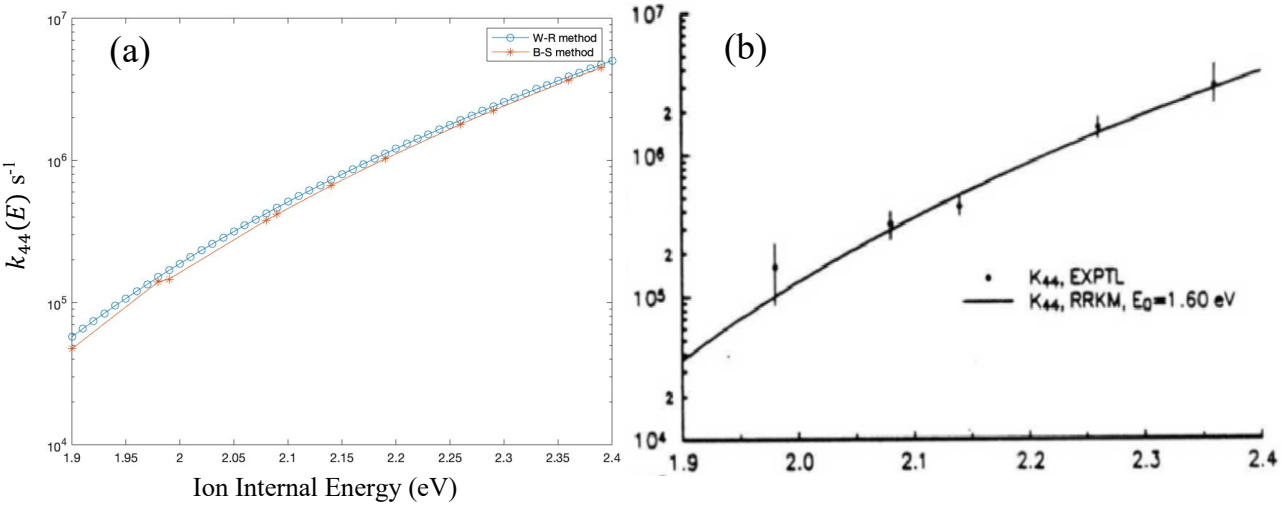

CHO – TS1 – k_{58}

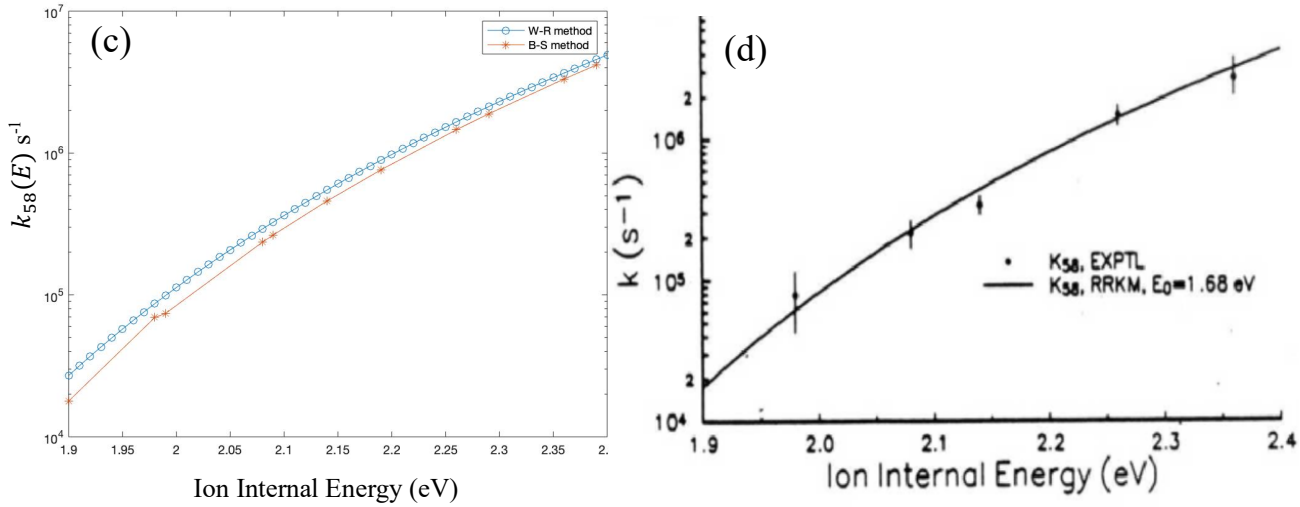

Figure 2: Comparison of my RRKM calculations to the results in ref [1]. (a) $k_{44}(E)$ with the WR and BS methods. (b) $k_{44}(E)$ from ref[1]. (c) $k_{58}(E)$ with the WR and BS methods. (d) $k_{58}(E)$ from ref[1].

Table 5: List of rate values k_{44} obtained in my RRKM calculations.

CH_3 – TS2 – k_{44}			
E_{int} (cm^{-1})	WR k_{44}	BS k_{44}	% difference
15325	57390	47272	17.6
15970	150934	140097	7.2
16050	168665	146092	13.4
16776	423364	378652	10.6
16857	465283	417538	10.3
17260	731022	665123	9.0
17664	1113925	1026535	7.8
18228	1921400	1794611	6.6
18470	2393092	2246942	6.1
19035	3879868	3683203	5.1
19277	4718697	4497653	4.7
CHO – TS1 – k_{58}			
E_{int} (cm^{-1})	WR k_{58}	BS k_{58}	% difference
15325	27012	17866	33.9
15970	86785	69324	20.1
16050	99030	74045	25.2
16776	291809	235454	19.3
16857	325640	264636	18.7
17260	549004	459384	16.3
17664	890225	762231	14.4
18228	1656661	1459780	11.9
18470	2124618	1890678	11.0
19035	3664802	3327395	9.2
19277	4566360	4176184	8.5

Interestingly, the Whitten-Rabinovitch and Beyer-Swinehart RRKM calculations deviate from the ref[1] curve by similar margins, but in opposite directions (see Table 4 and Fig. 2). The Whitten-Rabinovitch rates are higher than ref[1], whereas the Beyer-Swinehart rates are lower.

There are two differences between my calculations and those of ref [1]. First is the method employed to calculate the states/ density of states— I used the Whitten-Rabinovitch and

Beyer-Swinehart methods, whereas ref[1] used the algorithm of steepest descent. The second difference is that my calculations included rotational contributions to the rate constant, i.e.

$$\frac{Q_R^{\pm}}{Q_R} = \left(\frac{I_A^{\pm} I_B^{\pm} I_C^{\pm}}{I_A I_B I_C}\right)^{1/2}$$

This constant is greater than unity and therefore shifts my RRKM WR and BS calculations higher by a constant factor (1.0751 for TS1 and 1.2483 for TS2) compared to the ref[1] calculation that does not include this factor. With the rotational component included, the WR method differs more significantly from ref[1] than the BS method (Table 4). In other words, the WR and BS methods straddle ref[1]'s steepest decent method, but the WR is higher than the BS is lower. If the rotational component is removed from my calculations, the WR and BS methods would still straddle ref[1]'s algorithm of steepest decent, but more evenly. Therefore, it can be concluded that the researcher's algorithm of steepest decent slightly overcounted the states with respect to the more accurate Beyer-Swinehart direct-counting algorithm.

As seen both in Fig. 2 and Table 5, the Whitten-Rabinovitch method consistently overcounts states and densities compared to the more accurate Beyer-Swinehart direct-counting algorithm across the entire energy range. The disparity between the two methods is highest at small internal energies, and the gap shrinks significantly at higher energies. It is common for approximate methods to overcount at low energies (ref[2]). In my calculations, the smallest energy input corresponds to the larger-barrier TS1 (CHO) for $N^{\pm}(E - E_0)$, where $E - E_0 = 1.9\ eV - 1.68\ eV = 0.22\ eV$, or 1774 cm^{-1}. This low-energy input yields the greatest disparity between $N^{\pm}$ as counted by the Whitten-Rabinovitch (= 9966) vs the Beyer-Swinehart method (= 6638). Indeed, the higher barrier of TS1 is the reason the two methods deviate more for TS1 than TS2, across the entire energy range (see '% difference' column in Table 5).

References:

[1]: Riley, John, and Tomas Baer. "Unimolecular decay of energy-selected dimethylformamide cations: a combined molecular orbital and RRKM analysis." *The Journal of Physical Chemistry* 97.2 (1993): 385-390.
[2]: Moon, Jeong Hee, Meiling Sun, and Myung Soo Kim. "Efficient and reliable calculation of rice-ramsperger—kassel-marcus unimolecular reaction rate constants for biopolymers: Modification of beyer-swinehart algorithm for degenerate vibrations." *Journal of the American Society for Mass Spectrometry* 18.6 (2007): 1063-1069.

Section 5: Appendix

1. Matlab script used for the Whitten-Rabinovitch method:

```
%calculation for TS N(E-E0)
freq=[2986      2984    2965    2964    2880    2879    1750    1535    1467    1465
1456    1449    1435    1421    1219    1140    1118    1100    921     909     848
648     558     348     318     261     163     154     96];
energy = 1.9:0.01:2.4;
e0=1.68;
e=2227;
eVpercm=8065.544;
e0=e0*eVpercm;
energy = energy.*eVpercm;
s=length(freq);
N=length(energy);

ts_energy = energy - e0;
zpe=0.5.*sum(freq);
beta = ((s-1)/s)*mean(freq.^2)/(mean(freq)^2);

eprime=ts_energy./zpe;
w=zeros(1,N);
for i =1:N
    if eprime(i)<1
        w(i) = 1/(5.00*eprime(i)+2.73*sqrt(eprime(i))+3.51);
    else
        w(i) = exp(-2.4191*eprime(i)^0.25);
    end
end

a=1-(beta.*w);
Num_states_ts = ((ts_energy + a.*zpe).^s)/(factorial(s)*prod(freq));

%New calculation for parent ion "_p"
freq_p=[3019    3006    2975    2951    2945    2878    2870    1473    1468    1450
1445    1437    1415    1367    1260    1176    1121    1086    1056    939     903
899     699     549     394     360     310     210     118     85];
s_p=length(freq_p);
zpe_p=0.5.*sum(freq_p);
beta_p = ((s_p-1)/s_p)*mean(freq_p.^2)/(mean(freq_p)^2);

eprime_p=energy./zpe_p;
w_p=zeros(1,N);
for i =1:N
    if eprime_p(i)<1
        w_p(i) = 1/(5.00*eprime_p(i)+2.73*sqrt(eprime_p(i))+3.51);
    else
        w_p(i) = exp(-2.4191*eprime_p(i)^0.25);
    end
end
a_p=1-(beta_p.*w_p);
dw_p=zeros(1,N);
for i =1:N
    if eprime_p(i)<1
        dw_p(i) = -(5+(2.73/2)*eprime_p(i)^(-0.5))/((5.00*eprime_p(i)
+2.73*sqrt(eprime_p(i))+3.51)^(2));
    else
        dw_p(i) = -2.4191*0.25*eprime_p(i)^(-0.75)*exp(-2.4191*eprime_p(i)^0.25);
    end
end
density_p = (1-beta_p.*dw_p(i))*((energy + a_p.*zpe_p).^(s_p-1))/
(factorial(s_p-1)*prod(freq_p));

plank_cm=eVpercm*4.13566E-15;
rate = (33851.4/31487.9).*Num_states_ts./(plank_cm.*density_p);
```